

Highlights

External charged debris in a flowing plasma : charge fluctuation induced complexity

Bikramjit Joardar, Hitendra Sarkar, and Madhurjya P. Bora

- **Model:** Investigates the effect of periodic charge fluctuation of external debris in a flowing $e-i$ plasma.
- **Nonlinear complexity:** Demonstrates emergence of debris charge-dependent chaos and nonlinear Landau damping (NLLD) using kinetic and fluid simulations.
- **Nonlinear modeling:** Theoretical analysis confirms simulation findings.
- **New insights:** Positively charged debris induces stronger localised chaos compared to negatively charged debris, with latter exhibiting NLLD.
- **Potential application:** Findings offer new insights into the plasma-debris interactions which may add another dimension to the debris detection scenario in low Earth orbit plasma.

External charged debris in a flowing plasma : charge fluctuation induced complexity

Bikramjit Joardar, Hitendra Sarkar, and Madhurjya P. Bora*

Physics Department, Gauhati University, Guwahati, 781014, Assam, India

Abstract

In this work, we investigate the response of a flowing $e-i$ plasma to embedded external charged debris, focusing on the periodic debris charge fluctuations that can trigger complex phenomena such as chaos and nonlinear Landau damping. We employ both kinetic and fluid simulations to analyse the plasma response to the time-dependent debris charge. Our findings indicate that the nature of nonlinear response can be considerably different for fluctuating positively charged external debris from a negatively charged debris. The simulations show that the debris charge fluctuation causes damping of the ion-acoustic wave as the debris velocity nears the ion-acoustic speed through nonlinear Landau damping and wave-wave interactions. We also present a theoretical framework to support the simulation findings. Our findings provide critical insights into debris-plasma interactions which may be useful in applications involving space debris management.

Keywords: Plasma-Debris Interaction, Charge Fluctuation, Chaos, Nonlinear Landau damping

1. Introduction

Impurities or external entities in a typical electron-ion plasma is not a new subject and the arena of scientific research involving such “foreign” entities in plasma environments is dotted with numerous studies, which essentially began with Irving Langmuir’s pioneering work on plasma sheath in the 1920s and 1930s [1, 2, 3, 4, 5, 6]. One of the most distinctive branches which stemmed out of such plasma physics research is the so-called “dusty plasma”, which has become one of the core research areas in plasma physics [7, 8, 9, 10]. Another such area, which came to the notice of the scientific community is the interaction of the plasma with charged external or foreign bodies, when the importance of scientific studies of such interactions was realised during the early days of space exploration, in the 1960s, when several space missions began studying how satellite and spacecraft interact with space plasma environments [11, 12, 13, 14]. In

*Corresponding author: mpbora@gauhati.ac.in

recent years, research in this area has really accelerated, especially after the subject of space debris in relation to the safety of the satellites and space stations in low Earth orbits (LEOs) has been recognised as an important research area. Usually, space debris at LEO are detected with satellite and ground-based sensors operating at optical and radio ranges and these methods are not effective in detecting smaller debris (size $\lesssim 1$ cm) [15], though NASA's Haystack Ultrawide-band Satellite Imaging Radar (HUSIR) has been able to provide a map of LEO debris down to ~ 5.5 mm [16]. Recent techniques, based on detection of plasma oscillations excited by these smaller debris, have been tested successfully to detect some of these debris [17]. In essence, the number of proven and effective methods to detect these smaller debris, is by no means complete and we continue to look toward understanding different physical manifestations of plasma-debris interaction. And this work is an effort to understand the intricacies of these interactions by allowing more realistic physical conditions.

In recent times, our understanding about plasma-debris interaction has been steadily progressing due to several theoretical, experimental, and numerical studies [18, 19, 20, 21, 22, 23]. It is now definitively proved both theoretically and through numerical simulations that depending on the nature of the charged debris, different nonlinear waves in the ion-acoustic regime can get excited by moving debris [21, 23]. While we usually see dispersive shock waves due to a positively charged external debris, pinned solitons are formed due to phase space trapping through ion-ion counter streaming instability (IICSI) for a negatively charged debris [23]. Some very recent laboratory and numerical simulation studies have looked into the plasma-debris interaction in multi-ion plasma [22]. Several other studies have focused on shape, dimension, and speed of the debris on the propagation of these solitons theoretically and with experiments [24, 20], as well as bending and acceleration [25], damping (both collisional and Landau) [26] of the excited structures.

In this work, we plan to explore a yet unexplored area related to plasma-debris interaction by allowing the charge in the external debris to vary over time along with the presence of a stochastic component. There are good reasons as to why the charge on external debris should vary. Some seemingly plausible causes are periodic photoemission due to eclipse transitions (especially debris in the LEO), passage of the debris through the regions of density and/or temperature gradient of the ambient plasma, plasma wave interactions, intrinsic forcing due to spin or tumbling motion of the debris, and external modulations viz. during spacecraft remediation processes, among others. Out of these scenarios, the most important one is perhaps the debris charge modulation due to plasma wave interactions as this is an inherent process and possibly cannot be avoided. Debris moving at or near ion-acoustic speed is expected to make the charge on debris oscillate in time at ion-plasma frequency (ω_{pi}), through ion-acoustic wake oscillations [27]. As an ion-acoustic wave (IAW) passes over the debris, it periodically alters the ion and electron densities. Since the ion and electron currents depend sensitively on these densities, the wave creates an imbalance in the ion and electron fluxes to the debris surface. This imbalance, in turn, disturbs the equilibrium floating potential of the debris and the debris charge

adjusts dynamically to restore the balance, leading to a periodically oscillating debris charge. So, basically IAWs excited by the external charged debris, itself can cause the periodic fluctuation of the debris charge at frequencies $\sim \omega_{pi}$, which is very much inherent to the debris-plasma interaction scenario. This process is very much similar to the process of dust-charge fluctuation in a dusty plasma [27, 28]. This inherent charge fluctuation of the debris can be thought to be a forcing term, which can result in parametric coupling and can give rise to a wide range of nonlinear phenomena including chaos, sheath instability, nonlinear Landau damping [29] (NLLD) and can also affect the local turbulence. In this analysis, we primarily focus on two effects – chaos and NLLD, the signatures of which are most prominent. While detecting chaos is pretty straight forward, the same is not true for NLLD, which requires more than one confirmation methods. We believe that the periodic oscillation near ω_{pi} can trigger NLLD, which can then limit the wave amplitude, providing a feedback mechanism on the charging process and may eventually affect the nonlinear structures [30]. On the other hand, as chaotic oscillations can imply the breakdown of coherent wave-particle energy exchange, it can act as a probe for the wave-particle interaction limit [31, 32]. We carry out our primary investigation with a 1D electrostatic particle-in-cell (PIC) method [33]. We shall also use the results of a flux-corrected-transport (FCT) method [34] to support our findings.

1.1. Why 1D?

While the real physical system is invariably 3D, one can get valuable physics information from 1D models very easily. There are three pressing reasons why in many cases, we resort to a 1D modeling. First, the symmetry. As there is no preferential direction, any direction is equivalent. Second, in many cases, the dominant dynamics happen only in one direction viz. direction of the flow. So, one can analyse the essential physics from studying the system in that dominant direction only. The third and the most important is the ease of calculation in 1D models as compared to 2D or 3D. In 2D or 3D, the resolution required to resolve Debye-scale fluctuations in the vicinity of the external debris will be prohibitively large.

In our case, as we shall see, the major dynamical activities are along the longitudinal direction or the direction of plasma (or debris) flow. So as long as we do not expect the transverse activities to affect the dynamics considerably (which is in our case), we can safely consider the 1D model. By assuming a slab-symmetric or axisymmetric configuration and a uniform plasma flow, the system effectively reduces to one dimension without significant loss of physical generality. Note that when an extended object (like a block or slab) move in a plasma, majority of the dynamics happen across the plasma-facing side of the debris, which is essentially like a 1D situation as all interactions across the plasma-facing side should be same. The situation would have been completely different had there been a magnetic field, which would have necessarily required transverse dynamics, thus forcing a multi-dimensional model.

Moreover, the 1D model allows us to use tractable mathematical techniques for analysing the chaos such as Lyapunov exponent analysis, Kolmogorov–

Arnold–Moser (KAM) theory, and finite time Lyapunov exponent (FTLE) maps, which would be analytically and computationally prohibitive in higher dimensions. Hence, the 1D approach is not only physically motivated but also essential for uncovering the fundamental mechanisms governing plasma-debris interactions, which can be later benchmarked in detail through 2D or 3D models (which is beyond the scope of this work). The 1D model thereby serves as a minimal yet powerful framework to isolate and study these nonlinear mechanisms.

1.2. Organisation of the paper

The paper is organized as follows. In Section II, we present the results of kinetic and fluid simulations with the help of our *h*-PIC-MCC and *m*FCT codes, respectively. In Section III, we provide a theoretical analysis of the results obtained in Section II. We provide an additional analysis of the results obtained in earlier sections, in terms of power spectrum analysis in Section IV. In Section V, we conclude. We also provide a brief analysis of the effect of fluctuation of debris charge on turbulent dynamics. In the Appendix, we discuss the validity of our kinetic model in the light of *e*-*i* collisions.

2. Simulation results

2.1. The premise

Though technically it should be possible to model a self-consistent periodic fluctuation of charge in external debris embedded in a plasma, in reality it is much harder to model it mathematically as it would naturally require calculation of collision cross-sections to exactly determine the electron and ion currents to the debris, which may not obey the much used orbit motion limited (OML) theory, usually used to calculate the currents. It may be further complicated by the extended and arbitrary shape of the debris. Besides, a self-consistent fluctuation will necessarily require a coupling of a circuit-like differential equation with the partial differential equations of the fluid model for the plasma, so that we shall require a charging equation like

$$\frac{dQ_d}{dt} = I_i(t) + I_e(t) + I_{\text{wave}}(t) + \dots, \quad (1)$$

to be coupled to the plasma fluid equations, where Q_d is the charge on the debris and $I_{i,e,\text{wave}}$ are the currents to the debris due to plasma ions, electrons, and the IAW. For a fluid simulation, the most challenging part would be to model the “wave” current. On the other hand, a PIC simulation may naturally model the I_{wave} term through kinetic effects, but it does not natively compute the above charging equation dynamically and would require some kind of approximation with a sheath and potential model around the debris. Besides, it would also require much higher grid resolution for realistic calculation of these currents to the debris. As a result, one would ideally need a hybrid approach of fluid and PIC methods to model these fluctuations self-consistently.

In order to avoid these complexities, we have chosen to model the periodic fluctuation of the charge on external debris through an “external forcing” equation for the debris charge density ρ_{ext}

$$\rho_{\text{ext}}(x, t) = \rho_0(x)\mathcal{F}(t), \quad (2)$$

where $\mathcal{F}(t)$ is the time-dependent part. This model can be seamlessly incorporated into a fluid as well as a PIC model and the results can be very efficiently compared. Besides, the controllable external forcing-like equation allows us to have a finer control on the fluctuation parameters and helps us isolate different nonlinear phenomena through controlled tuning. In what follows, we shall present results from two different simulation methods – PIC simulation and fluid simulation with a flux-corrected transport solver, which justifies these observations.

Our primary results are due to the PIC simulation as it incorporates all the kinetic effects and full nonlinearities and also model a realistic plasma situation. The FCT model is a reduced fluid model, results from which should largely support the PIC simulation results.

2.2. The plasma model

The 1-D e - i plasma system with Boltzmannian electrons is modeled with the following equations with an exclusive time-dependent external charge density for the debris,

$$\frac{\partial n_i}{\partial t} + \frac{\partial}{\partial x}(n_i v_i) = 0, \quad (3)$$

$$\frac{\partial v_i}{\partial t} + v_i \frac{\partial v_i}{\partial x} = -\frac{1}{m_i n_i} \frac{\partial p_i}{\partial x} - \frac{e}{m_i} \frac{\partial \phi}{\partial x}, \quad (4)$$

$$n_e = n_0 \exp\left(\frac{e\phi}{T_e}\right), \quad (5)$$

$$\epsilon_0 \frac{\partial^2 \phi}{\partial x^2} = e(n_e - n_i) - \rho_{\text{ext}}(t; x - v_d t), \quad (6)$$

where n_i and n_e are the ion and electron number densities respectively, v_i is the ion fluid velocity, p_i is the ion pressure, ϕ is the electrostatic potential, m_i is the electron mass, e is the electronic charge, ϵ_0 is the vacuum permittivity and T_e is the electron temperature. The last term in the Poisson equation, ρ_{ext} is the term due to external charged debris which is moving with respect to the bulk plasma at a constant velocity v_d . Note that depending on whether the debris is charged positively or negatively, $\rho_{\text{ext}} \gtrless 0$. The pressure for ions is treated as polytropic

$$p_i \propto n_i^\gamma, \quad (7)$$

where γ is the ratio of specific heats. The normalized model can be written as

$$\frac{\partial n_i}{\partial t} + \frac{\partial}{\partial x}(n_i v_i) = 0, \quad (8)$$

$$\frac{\partial v_i}{\partial t} + v_i \frac{\partial v_i}{\partial x} + \gamma \sigma n_i^{\gamma-2} \frac{\partial n_i}{\partial x} = -\frac{\partial \phi}{\partial x}, \quad (9)$$

$$n_e = e^\phi, \quad (10)$$

$$\frac{\partial^2 \phi}{\partial x^2} = n_e - n_i - \rho_{\text{ext}}(t; x - v_d t), \quad (11)$$

where the densities are normalised by the equilibrium plasma density n_0 , length is normalized by electron Debye length λ_D , time is normalized by the inverse of ion-plasma frequency ω_{pi} , plasma potential ϕ is normalized by (T_e/e) . The temperature is expressed in energy units and velocity is normalized by the ion-acoustic speed $c_s = \sqrt{T_e/m_i}$. The quantity σ is the ratio of ion to electron temperature and is usually $\ll 1$. In the above equations, the external charge density ρ_{ext} is also normalized accordingly.

We consider the external charge density to be either positive definite or negative definite, so that the charge in particular debris remains same (either positive or negative) while oscillating in time.

2.3. Kinetic model – PIC simulation

2.3.1. The PIC simulation

It is important for the general reader that we explain the basics of PIC simulation of plasma, though it is widely used and described in details in many good textbooks, especially one by Birdsall [33]. The dynamics modelled by PIC simulation is as per the Boltzmann-Vlasov (or simply Vlasov) equation [35]

$$\frac{\partial f_j}{\partial t} + \mathbf{u}_j \cdot \nabla f_j + \frac{q_j}{m_j} \mathbf{E} \cdot \nabla_{\mathbf{u}_j} f_j = 0, \quad (12)$$

where $j = i, e$ stands for ions and electrons, f_j are the respective velocity distributions, \mathbf{u}_j are the respective particle velocities, in contrast to fluid velocity v_i used in Eqs.(8-10), and \mathbf{E} is the plasma electric field. The operator $\nabla_{\mathbf{u}_j}$ is the gradient operator in the respective velocity space. In presence of non-zero collisional momentum exchange, the right hand side of the above equation must be replaced by a collision term (which is zero in our case). The fluid equations given by Eqs.(8-10) are nothing but differently weighted average of the Vlasov equation Eq.(12). While the Vlasov equation is fully kinetic, the fluid model loses out the kinetic effects (those effects which involves individual particle properties) due to the averaging. Naturally, the fluid model is an approximation to the kinetic model.

The crux of the PIC model lies in its ability to model a large number of real-life plasma particles (of each kind) through a computational particle (also known as so-called *super-particle*) [33], which greatly reduces the computation time. Unless we consider a very strongly coupled plasma, the PIC model proves

to be a very efficient method to model kinetic plasma phenomena [33]. The PIC model starts with distribution of the computational particles as per the given velocity distribution (which in our case, is a Maxwellian) on a grid, which is a 1D uniform grid in our case. Our particle distribution is spatially random and uniform. Once the particles are distributed, the electrostatic potential ϕ is calculated at the grid points through a nearest neighbour approximation [33, 36], which is then used to calculate the plasma electric field \mathbf{E} at the grid points through the relation

$$\mathbf{E} = -\nabla\phi. \quad (13)$$

This provides us with the force \mathbf{F} at the particle positions through $\mathbf{F} = q\mathbf{E}$, which is again interpolated through a nearest neighbour scheme [33, 36]. Once the force is obtained, the following equations are inverted subsequently to update new velocity \mathbf{u} and then new position \mathbf{x} ,

$$\frac{d\mathbf{u}}{dt} = \frac{\mathbf{F}}{m}, \quad (14)$$

$$\frac{d\mathbf{x}}{dt} = \mathbf{u} \quad (15)$$

and the cycle repeats.

2.4. Description of the simulation

In this section, we shall present the results of PIC simulation of the above-mentioned e - i plasma with a time-varying external charged debris. The simulation is carried out with our well-tested *hybird*-PIC-MCC code [36, 37, 38, 23], which has already been successfully applied to several electrostatic problems including plasmas with secondary electron emission, kinetic dust-ion-acoustic wave with ion-Landau damping effect, and e - i dusty plasma with external charged debris.

The plasma is assumed to have an e - i number density $n_{e,i} \sim 10^{16} \text{ m}^{-3}$, with electron temperature $T_e \sim 1 \text{ eV}$ and ion temperature $T_i \sim 0.01 \text{ eV}$. The simulation box is of length $L \sim 140\lambda_D \sim 0.01 \text{ m}$. The cell size for computation is $\sim 6.25 \times 10^{-6} \text{ m}$ which is equivalent to $\sim 0.05\lambda_D$, enough to resolve fine-scale, Debye-scale fluctuations. The simulation is being performed with periodic boundary conditions. The simulation time and the box length is adjusted, so that the nonlinearities in the neighbourhood of the debris are not affected by the boundaries. The code can handle any arbitrary-shaped external charge distribution of arbitrary strength which can be either positive or negative with time-varying charge density. We can either make the debris move across the plasma or vice versa – the results being same in either case. Computationally, as mentioned before, we model our time-varying charge density with the following function

$$\rho_{\text{ext}}(x, t) = \rho_0(x)[1 + \tanh\{\Delta \sin(\nu t)\}] + \rho_{\text{noise}}(t), \quad (16)$$

$$\rho_0(x) = \tilde{\rho}_0 e^{-x^2/w}, \quad (17)$$

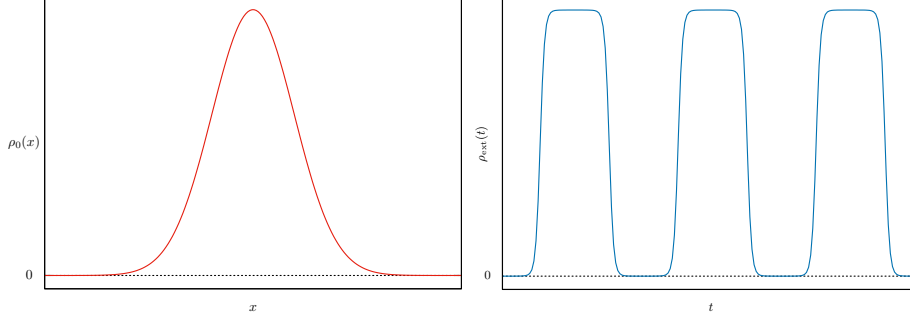


Figure 1: A schematic (not to scale) representation of the spatial distribution $\rho_0(x)$ (left) for the external charge and temporal variation of the distribution (right). These representations are without stochastic noise.

which is a spatially symmetric (Gaussian-like) charge distribution $\rho_0(x)$, oscillating in time. The parameter Δ is the *flatness* parameter of the time variation, ν is the oscillation frequency of the charge distribution, and w is the measure of spatial width of the distribution which is $\sim 2\lambda_D$, with $\tilde{\rho}_0$ denoting the peak of the debris charge density. It should be noted that the value of $\tilde{\rho}_0$ *must* be more than a critical value in order to sustain the debris-induced nonlinearity. In our case, with the present plasma parameters, the minimum $\tilde{\rho}_0^{(\min)} \sim 0.08$ with respect to the background charge density [23]. If it is not enough, the debris will be overwhelmed by the inherent noise in the system and the debris-induced effects will diffuse within a few plasma periods. The larger the value of Δ is, the steeper is the variation. Note that the $\rho_{\text{noise}}(t)$ part denotes a stochastic part of $\rho_{\text{ext}}(x, t)$, which adds a degree of random-ness to the oscillation.

2.4.1. Charge modulation

In Fig.1, we have schematically shown the spatial distribution of the external charge and its temporal variation (without noise). While the spatial distribution is a symmetric Gaussian, the distribution oscillates much like a top-hat function, oscillating between zero and some positive (or negative) value.

Or in other words, the charge distribution always remain positive or negative definite during the oscillation. The primary reason for choosing the oscillation is the way external debris get charged in the plasma. If we do not alter the debris properties (or plasma properties), the debris can get charged only in one way – either positive or negative, not both. One can, however get external debris charged in both ways if the mechanism of charging becomes completely different over time like the lunar surface. We know that the Moon acts like an external entity in the flow of solar wind plasma. During day-time, the lunar surface gets charged positively due to the solar UV radiation inducing photoemission of electrons from the lunar surface, while during night-time, the surface gets negatively charged. But, in our case, this fluctuation of charge on the debris is due to inherent plasma oscillations where there is no way that the charging mechanism can get changed within the oscillation time.

If we go a bit deeper, we see that the whole process of charging of external entities in a plasma is due to the asymmetric response of plasma electrons and positive charges toward the external surface. So, we can say that the top-hat-like fluctuation is rooted in the asymmetric response of the plasma.

2.4.2. Modeling of the noise

We treat the noise as one which can naturally arise in a plasma due to random fluctuations. If we denote the driving signal as $S(t)$, which in our case may be a periodic signal due to plasma wave, the total signal $T(t)$ can be thought to be composed of the signal $S(t)$ and a stochastic noise $R(t)$. However, we assume that the stochastic fluctuation is purely *environmental* i.e. it depends on the signal $S(t)$, so that the total signal can be written as

$$T(t) = S(t) + R(t), \quad (18)$$

where

$$R(t) = \begin{cases} R_0(t), & \text{if } S(t) = 0, \\ |\delta R(t)|S(t), & \text{if } S(t) > 0, \end{cases} \quad \delta R(t) < 0. \quad (19)$$

This model can be justified by considering the fact that even in the absence of any driving signal, the plasma continues to have background thermal fluctuations such as spontaneous Langmuir oscillations [39]. This explains the relation

$$T(t) = R_0(t), \quad \text{if } S(t) = 0. \quad (20)$$

On the other hand, when there is a driving signal (such as in our case), the plasma responds nonlinearly, which can be through nonlinear wave-particle interactions (viz. nonlinear Landau damping) [40, 41]. As this response is supposed to be dependent on the driving signal, we have

$$T(t) = S(t)[1 - |\delta R(t)|]. \quad (21)$$

Regarding the strength of the stochastic component, we have assumed it to be $R_0(t) \leq S(t)$ and $|\delta R(t)| \leq 1$. Though there is not any hard justification to this assumption, it is quite intuitive that stochastic fluctuations are always supposed to be lower than the driving signal, when the driving signal goes to zero and it always attenuates the signal, whenever it is non-zero [40, 41].

2.4.3. Chaotic dynamics

We are now going to discuss the chaotic dynamics induced by different oscillating external charge distributions.

The variable data (v_i, n_i) are extracted across the simulation domain as independent time series, which are then examined with Wolf's algorithm for possible chaotic nature. It is now well known that the Wolf's algorithm [42] applies Taken's theorem [43] to construct an m -dimensional phase space from a scalar time series $\{x_t\}$,

$$\mathbf{X}_t = [x_t, x_{t+\tau}, x_{t+2\tau}, \dots, x_{t+(m_{\text{PIC}}-1)\tau}], \quad (22)$$

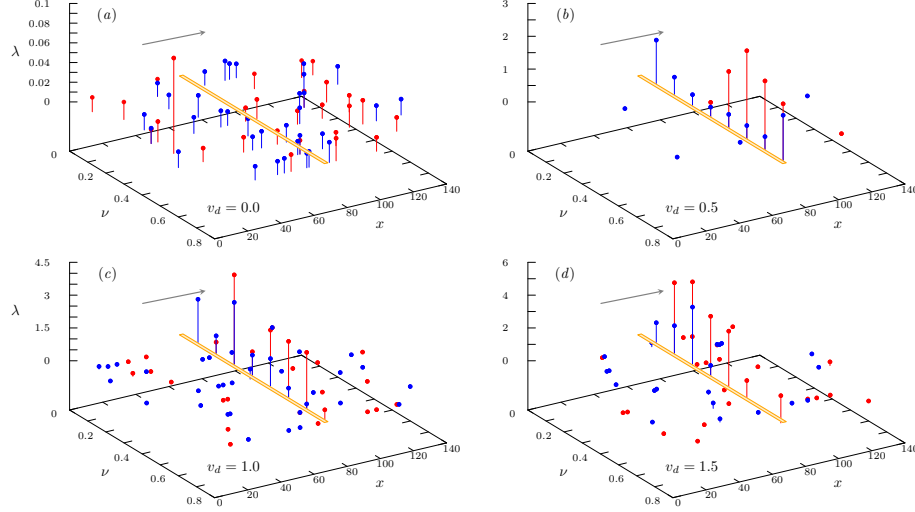


Figure 2: Maximal Lyapunov exponent λ , shown in the x - ν plane for a positively charged external debris (shown as the orange strip). The blue and red points indicate values of λ with and without stochastic fluctuation. The results are at time $\sim 20\tau_{pi}$. The arrow indicates the direction of debris velocity.

with m_{PIC} as the embedding dimension and τ as the time delay. The algorithm continuously measures the divergence between two nearest neighbour (forward in time)

$$\delta(t) = \|\mathbf{X}_t - \mathbf{X}'_t\|, \quad (23)$$

where \mathbf{X}'_t is \mathbf{X}_t 's nearest neighbour (in time). The so-called Lyapunov exponent [44], which is nothing but the exponential divergence of the nearest trajectories, is then calculated over *valid* divergence segments as

$$\lambda_j = \frac{1}{\Delta t} \ln \left[\frac{\delta(t + \Delta t)}{\delta(t)} \right], \quad (24)$$

where Δt is the time difference taken to compute the divergence. The maximal Lyapunov exponent is then calculated by

$$\lambda = \frac{1}{N} \sum_{j=1}^N \lambda_j, \quad (25)$$

where N is the number of valid divergence segments. Any positive λ indicates chaos and the further λ is away from 0, the stronger is the chaos. A typical rule of thumb is to have $\lambda \gtrsim 0.01$ for a definitive proof of chaos. In our case, we have used the variable n_i for the scalar time series $\{x_i\}$ and an embedding dimension $m_{PIC} = 4$ for our chaos test.

The result of the simulation is shown in Figs.2 and 3, where we have shown the scatter plots of λ in a x - ν plane. The position of the debris is indicated

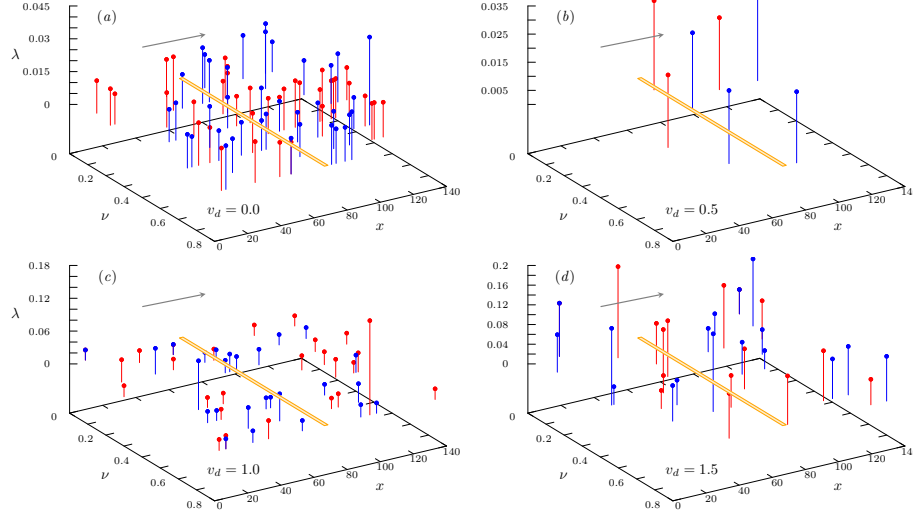


Figure 3: Maximal Lyapunov exponent λ , shown in the x - ν plane for a negatively charged external debris (shown as the orange strip). The blue and red points indicate values of λ with and without stochastic fluctuation as before. The results are at time $\sim 20\tau_{pi}$. The arrow indicates the direction of debris velocity.

by an orange-colored strip in the panels. The position is expressed in terms of electron Debye length λ_D and the frequency ν is expressed in terms of ion plasma frequency ω_{pi} . In order to help the perspective visualization of the value of λ , we have added “vertical drop-lines” from every point to the $z = 0$ baseline so that the length of the ‘drop-line’ indicates the value of λ . All simulation results are at time $\sim 20\tau_{pi}$, where τ_{pi} is the plasma period $= \omega_{pi}^{-1}$. The results for positively charged debris is shown in Fig.2 and that for negatively charged debris are shown in Fig.3. As we can see from Fig.2 that for positively charged debris, increase in debris velocity definitely induces quite stronger chaos in the oscillation, specifically at the site of the debris. The average strength of the λ in panel (a) is almost in the boundary line of chaos ~ 0.01 , which is without any relative motion between the plasma and external debris ($v_d = 0$). This should be contrasted with those in panels (b), (c), and (d), where we can see a definitive built up of chaotic oscillations. It should also be noted that the site of chaotic oscillation is mostly confined to the debris site. Besides, the stochasticity of fluctuation is not seen to have any systematic and correlated effect on λ , a situation which we shall explain later in Section 3.2.4.

In contrast to the positively charged debris, we can see a completely different scenario in case of negatively charged debris from Fig.3. In this case, we can see that the strength of the chaos is quite weak as compared to the chaos induced by fluctuating positively charged debris. Besides, the chaotic points are almost evenly distributed across the x - ν plane as opposed to the earlier case where the chaos is mostly confined to the debris site. As far as the effect of stochastic

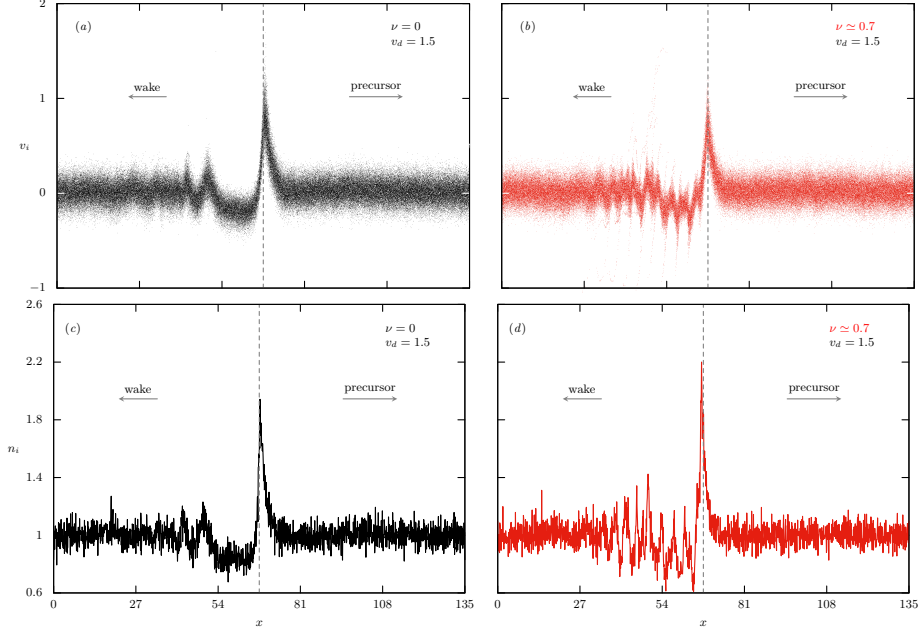


Figure 4: Ion phase space plots and ion density plots are shown in panels (a), (b) and (c), (d) for positively charged external debris. The left hand plots (black colored) are without any fluctuation of the debris charge and the right hand plots (red colored) are for periodic fluctuation of the debris charge. The value of the fluctuation frequency ν is given in each panel.

fluctuation is concerned, it is similar to that of positively charged debris.

The corresponding ion phase space and ion density plots are shown in Fig.4 for positive debris and in Fig.5 for negative debris. All frames of Figs.4 and 5 are drawn in the rest frame of the debris, which lies in the middle of the simulation window denoted by a dashed vertical line in each panel. The ion velocity is normalized to the ion-acoustic speed and the ion density is normalized by its equilibrium value. The length is normalized by electron Debye length λ_D . All these plots are without any stochastic fluctuation component. What we can see from the plots is that, the periodic charge fluctuation of the external debris has a minimal effect when the debris charge is negative, also manifested by weak chaos, as shown before.

2.5. Fluid model – FCT simulation

In this section, we shall try to model the fluctuation-induced chaos from a fluid perspective with flux-corrected transport simulation [21, 22]. Here, we use a multi-fluid FCT (*m*FCT) code based on Boris’s original algorithm [34] with Zalesak’s flux limiter [45], which we use to solve Eqs.(8-6) with time-varying ρ_{ext} . This code has also been extensively used to study debris-induced plasma wave phenomena [22].

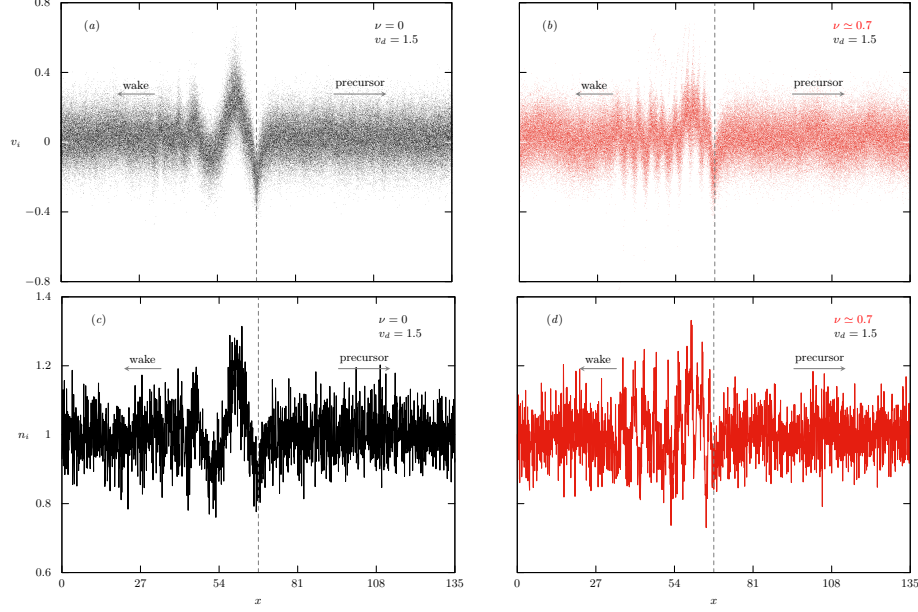


Figure 5: Ion phase space plots and ion density plots for negatively charged external debris. All other particulars are same as in Fig.4. The value of the fluctuation frequency ν is given in each panel.

The FCT formalism requires the hydrodynamic equations Eqs.(8-9) to be put in the form of a generalized continuity equation,

$$\frac{\partial f}{\partial t} = -\frac{\partial}{\partial x}(fv_i) + \frac{\partial s}{\partial x}, \quad (26)$$

where $f = (n_i, v_i)$ is the physical quantity to be solved, (fv_i) is the corresponding flux, and s is the source term. The external charged debris is entered through the Poisson equation Eq.(6) as before which is to be solved at each time step along with Eq.(26). The external charged debris is modeled with the same profile as used in the PIC simulation, given by Eq.(16).

We now present a full-spectrum Lyapunov exponent (LE) λ_k analysis of the velocity profile on the debris site, as obtained from FCT simulation. The algorithm to calculate Lyapunov exponent is based on Wolf's algorithm [42] for an embedding dimension $m_{\text{FCT}} = 6$.

$$\lambda_1 \geq \lambda_2 \geq \dots \geq \lambda_{m_{\text{FCT}}}, \quad m_{\text{FCT}} = 6, \quad (27)$$

for a scalar time series v_i , at the site of the debris, resulted out of the fluid simulation. We start by constructing the delay vectors

$$\vec{f}_j = [f(t_j), f(t_j + \delta t), \dots, f(t_j + (m_{\text{FCT}} - 1)\delta t)] \text{ in } \mathbb{R}^6, \quad (28)$$

required for phase-space reconstruction. The embedding dimension $m_{\text{FCT}} = 6$ is further verified through Kaplan-Yorke (KY) dimensional analysis [46] of the embedding dimension,

$$D_{\text{KY}} = j + \frac{\sum_{k=1}^j \lambda_k}{|\lambda_{k+1}|}, \quad \sum_{k=1}^j \lambda_k > 0, \quad (29)$$

where the summation is over all non-zero λ_k . This yields KY fractal dimension $D_{\text{KY}} \approx 5$ for our λ_k s which conforms to the general guideline $m_{\text{FCT}} > D_{\text{KY}}$, an over-conservation as compared to Taken's theorem [43] that in general requires $m_{\text{FCT}} > 2D_{\text{KY}}$. While calculating the Lyapunov spectrum, we have used a Theiler window [44] to avoid temporal correlation and tracked the divergence of the nearby trajectories using a linearized approximation. A Gram-Schmidt orthonormalization (i.e. QR decomposition) [47] is applied in each time step to the evolving tangent vectors and the LEs are calculated finally by

$$\lambda_k = \frac{1}{T} \sum_{p=1}^N \log R_{kk}^{(p)}. \quad (30)$$

In the above expression, R is the upper-triangular matrix as obtained from the QR decomposition, p is the index of time step at which the decomposition is carried out, N is total number of such steps, and T is the physical time $T = \sum_{k=1}^N \Delta t_k$ with Δt being the time interval (of the time series) between each decomposition step.

Note that the reason for the embedding dimension for FCT simulation ($m_{\text{FCT}} = 6$) being higher than that for PIC simulation ($m_{\text{PIC}} = 4$) can be understood by considering the presence of “noise” in PIC simulation, which is almost absent in FCT simulation as it numerically solves the model equations exactly. On the other hand, the “noise” in PIC simulation scales as inverse of the square root of total number of computational particles [48]

$$\text{PIC Noise} \propto \frac{1}{\sqrt{N_p}}, \quad (31)$$

where N_p is the total number of computational particles used in the PIC simulation. As computational cost per PIC cycle is $\propto N_p$, a decrease in “noise” by a factor of 2 increases computational cost by a factor of 4, making the option of increasing N_p not a viable one. Naturally, the FCT simulation can detect more fine-scale fluctuations whereas PIC simulation picks up more coarse-grained fluctuations which results in a low-dimensional dynamical system for PIC simulation.

The results of this analysis is shown in Fig.6, which shows the full spectrum LE. In the figure, the axes are the three dominant LEs ($\lambda_{1,2,3}$) and the red and blue circles respectively denote the cases $\rho_{\text{ext}} > 0$ and < 0 . Apart from the fact that all $\lambda_{1,2,3} > 0$ which signifies chaos, the accumulation of the red circles at the upper portion of the figure indicate a considerably stronger chaos for

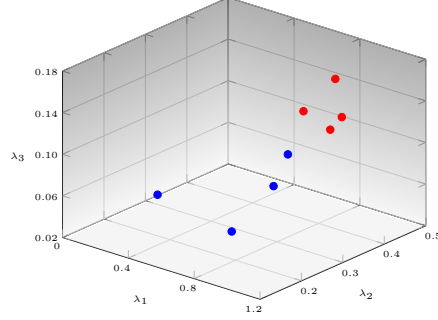


Figure 6: Full spectrum LEs calculated from the time series obtained from the FCT simulation.

$\rho_{\text{ext}} > 0$ than < 0 . The four cases corresponding to four circles in the figure (red and blue) are for different debris velocities $v_d = 0.2, 0.5, 1.0$ and 1.5 (the numerical code used to calculate the full-spectrum LE is available).

2.6. Nonlinear Landau damping?

We now present a combined result of PIC and FCT simulations which point out a phenomenon similar to what is known as “nonlinear Landau damping” [29]. In both cases, we observe a suppression of oscillations when $v_d \sim c_i$, where $c_i = \sqrt{T_e/m_i}$ is the phase velocity of the ion-acoustic oscillations. However, the fundamental physics behind this observation is slightly different in both cases.

Consider an external charged debris which is moving with a velocity v_d with a potential profile $\phi(x - v_d t)$, modulated by a time-varying charge $Q(t)$. The plasma responds to this debris field through ion-acoustic oscillations with a phase velocity c_i . So, when $v_d \sim c_i$, we have a resonant energy transfer between the background plasma and the charged debris. However, the oscillating charge of the debris is going to introduce another frequency scale $\sim \nu$. As a result, the Doppler-shifted frequency of the oscillation (as seen by the debris) is given by

$$\omega_{\text{forcing}} = \nu + k v_d. \quad (32)$$

Thus, we have a resonance condition, when $\omega_{\text{forcing}} \simeq \omega_{\text{IA}} = k c_i$, or

$$v_d \simeq c_i - \frac{\nu}{k}. \quad (33)$$

We can expect a strong wake when a resonance occurs and destructive interference when it becomes out of phase,

$$|\nu + k(v_d - c_i)| \gtrsim 0, \quad (34)$$

reaching a maximum of π when they become completely out of phase by a turnover time of τ_π

$$\tau_\pi |\nu + k(v_d - c_i)| \sim \pi. \quad (35)$$

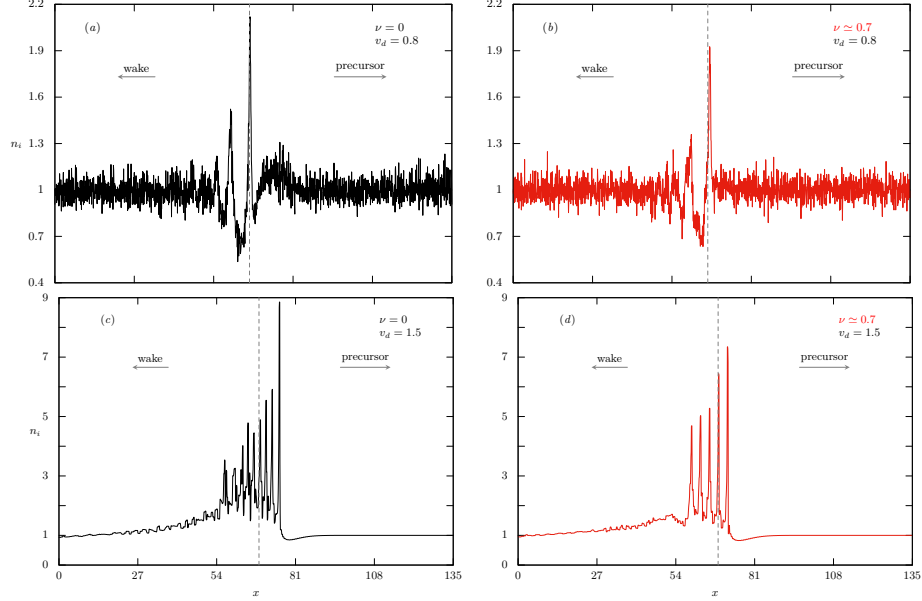


Figure 7: Suppression of density oscillations with periodic charge fluctuation of the negatively charged debris. The top panels (a), (b) are obtained from PIC simulation while the bottom panels (c), (d) are obtained from FCT simulation. The panels on the left are without any charge fluctuation and those on the right are with charge fluctuation. The vertical dashed line denotes the position of the debris.

It is then more likely that ‘anti-resonance’ occurs via relations (34) and (35) rather than a resonance condition occurs, which has to be exactly via relation (33). So, we expect a suppression of oscillations to occur, on average, due to the periodic variation of debris charge. This is the reason behind the observation of suppression of oscillation seen in the FCT simulation results. However, as the PIC simulation is expected to also incorporate the effect of NLLD, we perform an additional check on the ion velocity distribution function (VDF) as obtained from PIC simulation. Though there are no definitive proofs of NLLD in general, for collision-less electrostatic plasma such as ours, a flattening of the velocity distribution can be attributed to NLLD.

This effect is shown in Fig.7 for negatively charged debris, both as obtained from PIC and FCT simulations. However, this resonant suppression of oscillation occurs at $v_d \lesssim c_i$ for PIC simulation and at $v_d \gtrsim c_i$ for FCT simulation as can be seen from the figure. This discrepancy can be explained from the fact that the PIC simulation captures the full kinetic response including wave-particle resonance and phase space trapping while the FCT simulation captures only the macroscopic fluid-like wave-wave response and lacks phase mixing. In Fig.8, we have shown the ion VDF obtained from PIC simulation data with and without debris charge fluctuation, which clearly show the flattening of the VDF with fluctuation. The suppression of oscillations combined with the definitive

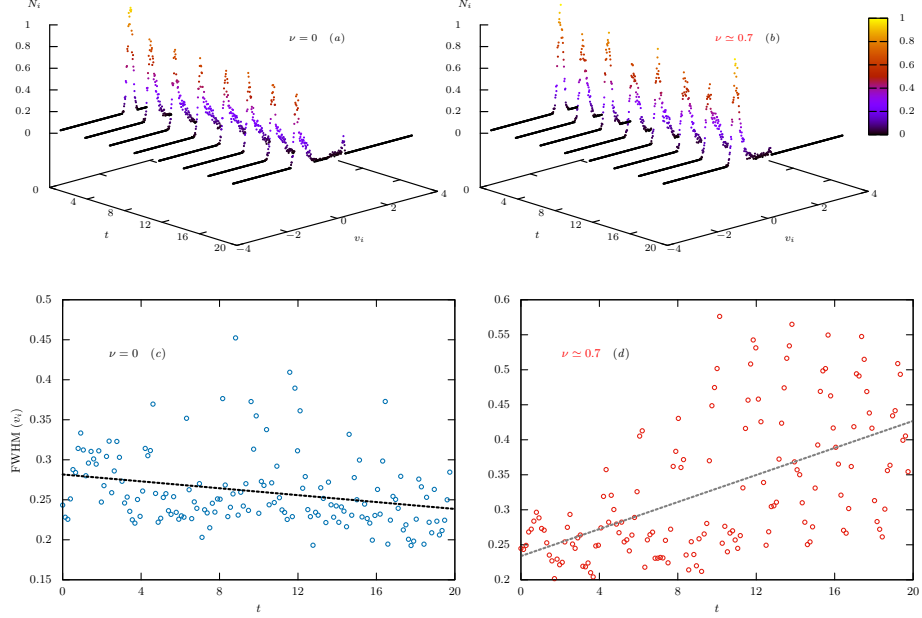


Figure 8: Flattening of the ion VDF due to charge fluctuation of the negatively charged debris. While the top panels (a) and (b) display respectively the VDFs calculated from the PIC simulation without ($\nu = 0$) and with ($\nu \sim 0.7$) fluctuation, the bottom panels (c) and (d) show the numerically calculated FWHMs for the corresponding VDFs. The panel (d) on the right clearly shows that the VDF is flattening due to fluctuation.

proof of flattening of the ion VDF in PIC simulation strongly supports the fact that oscillations undergo NLLD due to charge fluctuation in the case of negatively charged debris. We note here that this flattening of ion VDF is not seen in case of fluctuating positively charged debris. In the above analysis, we have used $v_d = 0.8$.

3. Theoretical analysis

3.1. Torus breakdown of a chaotic plasma model

In this section, we try to understand the theory behind the chaotic oscillation observed in the simulations and try to understand some of the observations related to stochastic fluctuations and why the properties of chaos for positively and negatively charged debris are fundamentally different. In particular, we shall discuss how the fluctuation of charge density of a debris may force the system to undergo torus breakdown [49, 31, 50] and become chaotic.

In order to facilitate a dynamical analysis, we make a coordinate transformation to the moving frame of the debris with the introduction of a scaled time $\tau = t - x/v_d$, so that in terms of the scaled variable we have $\partial/\partial t \rightarrow \partial/\partial \tau$ and

$\partial/\partial x \rightarrow -v_d^{-1}\partial/\partial\tau$ [38]. With this transformation, our plasma model represented by Eqs.(8-11) becomes

$$\frac{\partial n_i}{\partial\tau} - \frac{1}{v_d} \frac{\partial}{\partial\tau}(n_i v_i) = 0, \quad (36)$$

$$\frac{\partial v_i}{\partial\tau} - \frac{v_i}{v_d} \frac{\partial v_i}{\partial\tau} - \frac{\gamma\sigma}{v_d} n_i^{\gamma-2} \frac{\partial n_i}{\partial\tau} = \frac{1}{v_d} \frac{\partial\phi}{\partial\tau}, \quad (37)$$

$$\frac{1}{v_d^2} \frac{\partial^2\phi}{\partial\tau^2} = n_e - n_i - \rho_{\text{ext}}(\tau). \quad (38)$$

Integration of Eq.(36) gives us

$$n_i = \frac{v_d - v_0}{v_d - v_i}, \quad (39)$$

where v_0 is the velocity of the ions at infinity (or far away from the debris). In the above integration, we have also used the boundary condition that at ∞ , $n_i \rightarrow 1$. Note that for the above formalism to work, we must have $v_d \leq (v_0, v_i)$ or else the density would be negative, which is unphysical. Without loss of any generality we can assume $\gamma = 2$ which helps us to integrate Eq.(37) to have

$$\phi = \frac{1}{2} (v_0^2 - v_i^2) - v_d(v_0 - v_i) + 2\sigma \left(1 - \frac{v_d - v_0}{v_d - v_i}\right), \quad (40)$$

where we have used the expression given by Eq.(39). Inserting the above expressions in Poisson equation, we have the following nonlinear second order differential equation in v_i ,

$$\ddot{v}_i A + \dot{v}_i^2 B + C = 0, \quad (41)$$

where the ‘‘ refers to derivative in τ and

$$A = \frac{1}{v_d^2} \left(\mu_i - 2\sigma \frac{\mu_0}{\mu_i^2} \right), \quad (42)$$

$$B = -\frac{1}{v_d^2} \left(1 + 4\sigma \frac{\mu_0}{\mu_i^3} \right), \quad (43)$$

$$C = \rho_{\text{ext}}(\tau) + \frac{\mu_0}{\mu_i} - e^\phi \quad (44)$$

where $\mu_i = v_d - v_i$ and $\mu_0 = v_d - v_0$. Note that Eq.(41) is a highly nonlinear non-autonomous equation.

3.1.1. Torus breakdown

As we have mentioned that the system is highly nonlinear, it can undergo a chaotic transition with the variation of different control parameters. The fluctuation frequency ν of the charge density of the external debris and the debris velocity v_d are two such parameters. As we shall observe, the system makes several quick transitions from quasi-periodic to chaotic states and vice versa

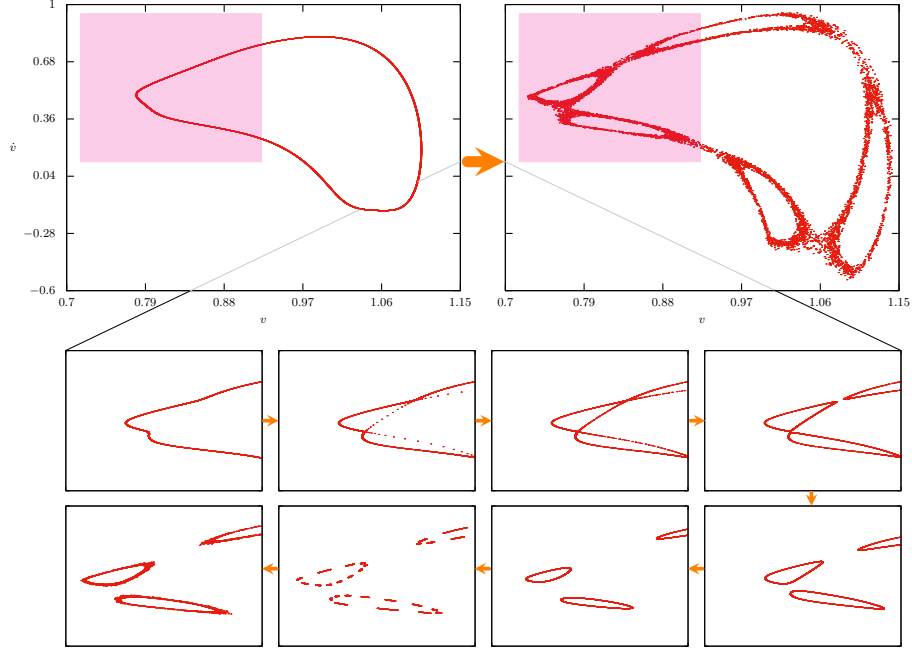


Figure 9: Poincaré plots of one transition phase from periodic to a chaotic state through torus breakdown. The initial (periodic) state is shown at the left top and the final chaotic state is shown at the right top panels. The arrow and the blown up transition phases are shown in the lower smaller panels.

when the control parameters are varied. So, there are several non-chaotic states of the system interspaced with numerous stages when the system undergoes torus breakdown and becomes chaotic. These breakdowns can be very quick and dramatic and do not follow a fixed pattern – a hallmark of torus breakdown [49, 31, 50]. One such transition phase is shown in Fig.9 through the Poincaré plots.

The charge fluctuation of the external debris is modeled by periodically switching the debris term on and off with a frequency ν . Toward this, the external debris term is expressed in a periodic top-hat function as mentioned before

$$\rho_{\text{ext}}(\tau) = \rho_0[1 + \tanh\{\Delta \sin(\nu\tau)\}], \quad (45)$$

where ρ_0 denotes of the strength of the charge density and Δ controls the steepness of the top-hat function which is typically $\sim 8 - 10$. As our system is normalized, ρ_0 is typically set to ~ 0.5 , which is about 50% of the background plasma density. The fluctuation frequency ν is set to $\sim 1 - 5$ or about five ion-plasma periods. In Fig.9, we have shown torus breakdown of the system where, in the top row, the Poincaré map of the initial deformed torus (quasi-periodic) is shown, which makes a final transition to a chaotic state on the right when the breakdown is complete. The successive transition from the initial state to the

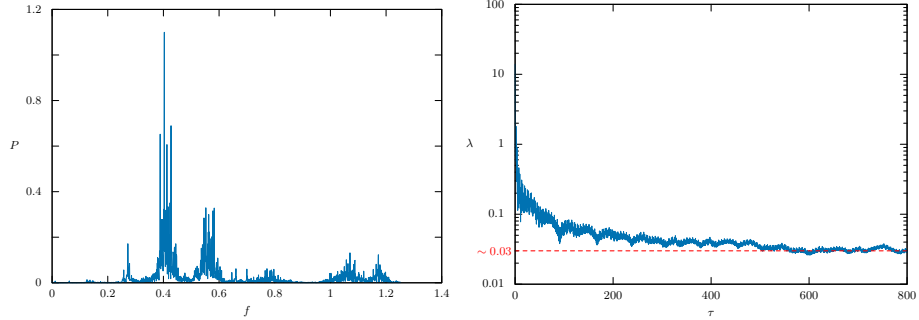


Figure 10: Power spectrum density at transition and maximal Lyapunov exponent at the final chaotic state.

final state is depicted in the smaller panels at the lower rows for shaded region marked in the bigger panels. The whole transition occurs within the interval of the debris velocity $v_d \in [1.596, 1.6]$. The torus breakdown is further confirmed by the power spectrum density P of the oscillation, shown in the left panel of Fig.10, where one can see the numerous random frequencies dominated by some prominent frequencies. The final chaotic state is also confirmed by the maximal Lyapunov exponent λ shown in the right panel of Fig.10, which settles down at about ~ 0.03 .

The reason for the *quick* transition to a chaotic regime in the case of PIC simulation compared to the analytical model is that the analytical model is a reduced fluid model, which does not have any kinetic effects and provides the dynamics for only a single fluid element. Whereas the PIC model inherently has all the possible kinetic effects such as nonlinear Landau damping, phase-mixing, and particle trapping and nonlinearities making it intrinsically fast and nonlinear. Besides, it shows the cumulative dynamics of millions of particles with many directions for making some of the Lyapunov exponents grow fast.

3.2. KAM tori analysis

We note that the Kolmogorov–Arnold–Moser (KAM) theory [51] describes how invariant tori exists in nearly integrable Hamiltonian systems. In typical cases, these invariant tori break up through destruction of homoclinic orbits (so-called homoclinic tangles) leading to chaos, which is known as torus breakdown [31, 50]. However, before we can qualify the nature of the chaos in our system as torus breakdown (seems possible from the numerical solutions from the previous section), we need some more clarifications in this regard.

3.2.1. Preliminary analysis

Let us write down our system represented by Eq.(41) in a generalized form

$$\ddot{x}A(x) + \dot{x}^2B(x) + C_0(x) + \epsilon f(\tau) = 0, \quad (46)$$

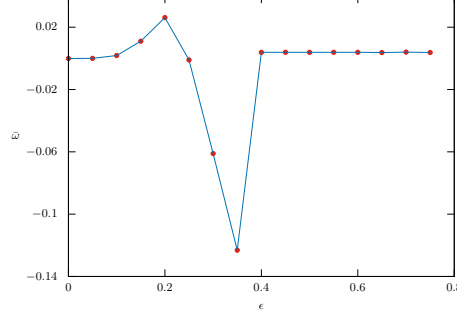


Figure 11: The frequency map signifying the transition to chaos through resonance.

where $x = v_i$ and the coefficient $C(x, \tau)$ is broken up into an autonomous and a time-dependent part

$$C_0(x) = \frac{\mu_0}{(v_d - x)} - e^{\phi(x)}, \quad (47)$$

$$\epsilon f(\tau) = \rho_{\text{ext}}(\tau). \quad (48)$$

Here, we have treated the external charged debris as a perturbation with a smallness parameter ϵ . The equivalent unperturbed planar system is given by

$$\begin{aligned} \dot{x} &= y, \\ \dot{y} &= F_0(x, y) = \frac{-y^2 B(x) - C_0(x)}{A(x)}. \end{aligned} \quad (49)$$

The equilibrium of the above system implies that $y = C_0(x) = 0$. So, the linearized Jacobian of the vector field (y, F_0) at a point $(x_s, y_s) \equiv (x_s, 0)$ in equilibrium is given by

$$J = \begin{pmatrix} 0 & 1 \\ J_{21} & 0 \end{pmatrix}, \quad J_{21} = -\frac{C'_0(x_s)}{A(x_s)}, \quad (50)$$

with the eigenvalues ϱ of the Jacobian as $\varrho = \pm\sqrt{J_{21}}$. The equilibrium point x_s can be determined from the condition $C_0(x) = 0$, and it comes out to be $x_s \simeq 1.05935$, which shows that $J_{21} < 0$ and the existence of a saddle point and a homoclinic orbit can be ruled out for the unperturbed system [52]. Apparently Eq.(41) is a highly nonlinear system and as it contains a \dot{v}_i^2 term, it is not likely to be reducible to a Hamiltonian system as well, even in the extended phase space (v_i, \dot{v}_i, τ) . This is also obvious from the fact that the flow is ‘non volume-preserving’ i.e. $\nabla \cdot \dot{\mathbf{x}} \neq 0$, where $\mathbf{x} = (x, y)$, which can be readily found out by observing that

$$\nabla \cdot \dot{\mathbf{x}} \equiv \frac{\partial \dot{x}}{\partial x} + \frac{\partial \dot{y}}{\partial y} = -2y \frac{B(x)}{A(x)} \neq 0. \quad (51)$$

All these facts indicate that a typical breakdown of KAM tori is *not* possible in our system. However, strong signature of torus breakdown suggests that

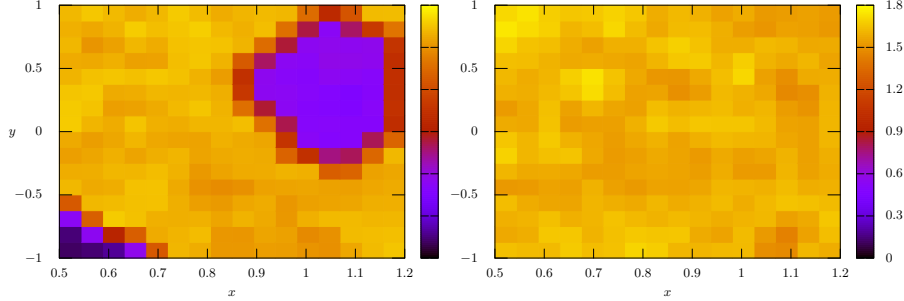


Figure 12: The FTLE maps for positive forcing (left) and negative forcing (right).

torus breakdown may still occur, though not through tangles but via shear and resonance [53, 54, 55]. This insight leads us to carry out an analysis through frequency and finite-time Lyapunov exponent (FTLE) maps [56, 57] in the next subsection. The above analysis also shows that the system does not preserve phase space volume and dynamically acts like a dissipative system though physically it does not have any dissipation.

3.2.2. Frequency and FTLE maps

We now express our external charged debris term as a perturbation, as mentioned before $\rho_{\text{ext}}(\tau) = \epsilon f(\tau)$, where ϵ is small but ≥ 0 , depending on the nature of charged perturbation. In order to compute the frequency map, we consider the actual time evolution of $x(\tau)$, as obtained from the numerical solution of Eq.(46) which is always real. From this, we construct the analytic (or complex) signal $z(\tau)$ by incorporating the Hilbert transform $\mathcal{H}[x(\tau)]$ of $x(\tau)$,

$$z(\tau) = x(\tau) + i\mathcal{H}[x(\tau)], \quad (52)$$

This helps us compute the instantaneous frequency $\omega(\tau)$

$$\omega(\tau) = \frac{d}{d\tau}\theta(\tau), \quad \text{where } \theta(\tau) = \arg[z(\tau)]. \quad (53)$$

We however use the average instantaneous frequency $\bar{\omega}$, averaged over a certain time T to cancel out the transient fluctuations

$$\bar{\omega} = \frac{1}{T} \int_{T_0}^T \omega(\tau) d\tau. \quad (54)$$

In Fig.11, we show a plot of $(\bar{\omega}, \epsilon)$ with $\epsilon > 0$ (positive charge perturbation) for a region of torus breakdown, shown in Fig.9. The figure shows that in the region $\epsilon \lesssim 0.2$ and $\gtrsim 0.4$, the instantaneous average frequency varies smoothly signifying quasi-periodic motion. In the region $\epsilon \simeq 0.25 - 0.35$, we have a sharp transition as well as some fluctuations indicating the onset of chaotic motion, which indicates a torus breakdown with possible resonance.

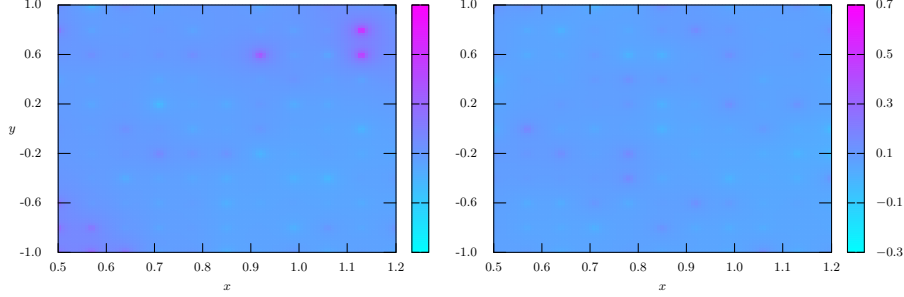


Figure 13: The FTLE difference maps showing effect of stochastic fluctuation for positive forcing (left) and negative forcing (right).

In order to compute the FTLE maps, we compute the Lyapunov exponent by calculating the divergence of orbits over a finite time window T , giving the FTLE [56, 57]

$$\lambda_T(\mathbf{x}_0) = \frac{1}{T} \log \frac{\|\delta(T)\|}{\|\delta(0)\|}, \quad (55)$$

where $\delta(0)$ is the initial separation of two nearby trajectories and $\delta(T)$ is the separation of the orbits at time T . We note that the maximal Lyapunov exponent can be recovered through $\lambda_{\max} = \lim_{T \rightarrow \infty} \lambda_T(\mathbf{x}_0)$. The two FTLE maps – one for positive charged perturbation and the other for negative, are shown in Fig.12. As we can see that for positive charge perturbation (positive forcing with $\epsilon = +0.1$), there are dark basins with very low FTLEs on either sides with surrounding yellow-orange colored high-FTLE region. This sharp contrast is a definitive signature for large lobes of mixing of tori, indicating a torus breakdown. On the other hand, negative charge perturbation (negative forcing with $\epsilon = -0.1$) does produce chaotic regions but as we can see from the right panel, the map is more or less uniform. The FTLE maps further confirm our earlier speculation that a positive charged perturbation produces very pronounced fractal scattering indicating stronger chaos while a negative charge perturbation of the same amplitude produces a milder chaos.

3.2.3. Perturbation-dependent chaos

It is now amply clear from the numerical as well as theoretical analyses that the chaotic behavior of the plasma system with external charged debris is highly dependent on the nature of the charged debris (positive and negative). Physically, we can perhaps understand it by rewriting Eq.(41) as

$$A(v_i)\ddot{v}_i = -\dot{v}_i^2 B(v_i) - C(v_i, \tau), \quad (56)$$

which represents the total force of the system with $A(v_i)$ acting as a mass. As $C(v_i, \tau) = C_0(v_i) + \rho_{\text{ext}}(\tau)$, total forcing is larger when $\rho_{\text{ext}}(\tau) > 0$, while the forcing is reduced when $\rho_{\text{ext}}(\tau) < 0$ with a possibility of even cancelling the force rendering the system to a force-free state. So, positive charge perturbation

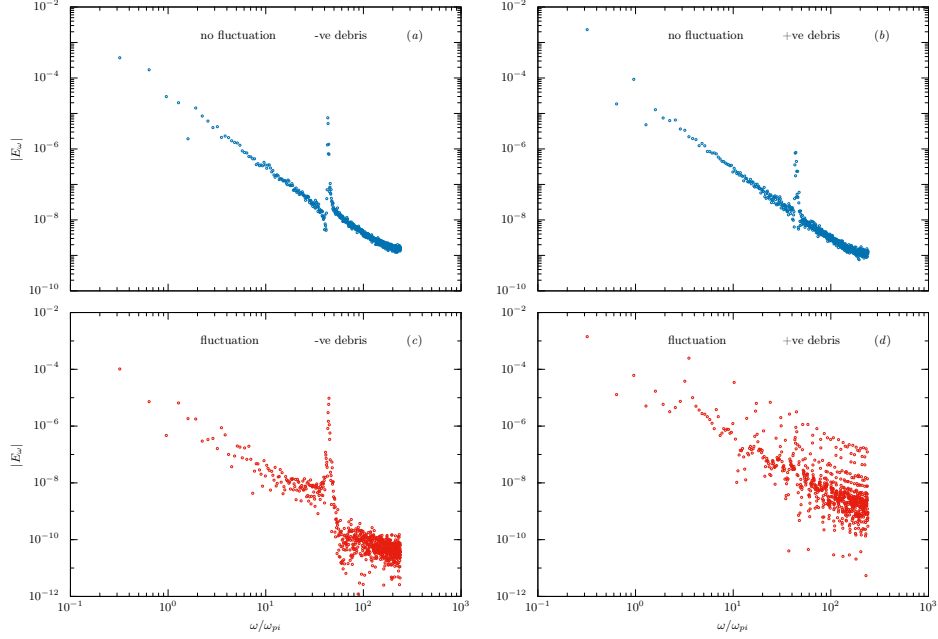


Figure 14: The ion energy spectrum $|E_\omega| \sim (v_i^2)$ for both negatively and positively charged debris with and without fluctuation. The upper blue colored panels (a) and (b) are for negatively and positively charged debris, respectively without any periodic charge fluctuation of the debris. The lower red colored panels (c) and (d) are for negatively and positively charged debris with periodic charge fluctuation of the debris.

pushes the system away from an equilibrium which results in a stronger chaotic state.

3.2.4. Effect of stochastic fluctuations

In practice, we would generally expect a stochastic component to the fluctuating charge density of the external debris, which can be modeled as a noise to the $\rho_{\text{ext}}(\tau)$

$$\rho_{\text{ext}}(\tau) = \rho_{\text{det}}(\tau) + \epsilon_{\text{noise}}\xi(\tau), \quad (57)$$

where ϵ_{noise} denotes the strength of the noise (or stochastic part) while the first term denotes the deterministic part. In Fig.13, we show the FTLE difference maps for two cases $\epsilon = \pm 0.1$ where the difference between the usual FTLE and one with stochastic component is shown. We can see from the figure that in both cases ($\epsilon = \pm 0.1$), the noise tends to destabilize weakly regular (non-chaotic or marginally chaotic) areas, whereas highly chaotic zones are least affected. So, stochastic forcing primarily affects the marginal or near-integrable areas and overall chaotic property of the system remains broadly same, a result which is confirmed from our PIC simulation.

4. Spectral signature of the phase space dynamics

In this section, we provide an analysis on the basis of spectral signatures of the chaotic phase space dynamics from the PIC simulation data. The analysis broadly confirms our earlier observations given in Sections 2 and 3. In Fig.14, we have shown the ion energy spectrum $|E_\omega| \sim (v_i^2)$ for both negatively and positively charged debris with and without debris charge fluctuation. The first observation is that the energy spectra becomes flattened at higher frequencies which points to the energy redistribution among the waves and particles due to linear and NLLD [29, 58, 59]. We note that the system has no physical dissipation which would have steepened the spectra at the right ends indicating loss of energy. However, in absence of any physical dissipation, the Landau damping merely redistributes the energy keeping the total energy content of the system to remain constant, which causes this flattening.

The other important observation is the broadening of the spectrum in presence of periodic charge fluctuation of the debris. This broadening indicates that the coherent cascading of energy is no longer possible when there is a periodic charge fluctuation of the debris. This also points toward the limitation imposed by chaotic oscillations on coherent transfer of energy from wave to particle and vice versa. The higher broadening of the spectrum for fluctuation of positively charged debris [panel (d)] indicates more loss of coherence due to a stronger chaos [60, 61]. These energy spectra also suggest that the nonlinear structures produced due to negatively charged debris are dynamically more robust and are less prone to any charge fluctuation of the debris.

The spike at $\omega \sim 43\omega_{pi}$ in the spectra is due to the electron plasma frequency which basically shows that the primary driven mechanism of the ion oscillation is due to the electron response.

5. Conclusions

In this work, we have looked into the dynamics governing the interplay between external charged debris and a flowing $e-i$ plasma with a particular emphasis on the role of the periodic fluctuation of debris charge. Our analysis is focused on how these fluctuations, introduced as an external forcing in our model, affect the plasma response. We note that periodic charge fluctuation on external debris can occur naturally due to a feedback response to the IAW induced by the presence of the external debris. Our analysis shows emergence of complex nonlinear phenomena including the emergence of chaos and the manifestation of NLLD.

We took a dual simulation approach to unravel these dynamics using a kinetic particle-in-cell (PIC) simulation and flux-corrected transport-based (FCT) fluid simulation. Our findings reveal that the charge polarity of the debris plays a crucial role in determining the system's behaviour. The charge fluctuation of the debris is implemented through a periodic external forcing model in both the simulations with the charge polarity fixed as either positive or negative throughout the simulations. Some key findings of our simulations are:

- The debris charge fluctuation acts as the trigger for chaotic oscillations, regardless of the charge polarity and the relative velocity between the plasma and debris.
- For a positively charged debris, we have observed a much stronger chaotic response confined at the debris site, with the maximal Lyapunov exponent increasing with the debris velocity. In contrast, negatively charged debris creates a more uniform weak chaos pattern across the domain.
- When the frequency of debris velocity approaches IA speed $v_d \sim c_i$, both PIC and FCT simulations detect damping of the nonlinear wave, which can be due to both nonlinear wave-particle resonance (NLLD) as well as nonlinear wave-wave interactions. However, while FCT simulation can only show wave-wave interactions, PIC simulation can show both the effects. The existence of NLLD is validated from the flattening of the ion velocity distribution.
- The added stochastic component to the regular periodic fluctuation does not affect the chaotic ion-acoustic oscillations significantly.

Theoretically, we have shown that the emergence of chaos due to the periodic charge fluctuation of the debris is through torus breakdown, though the breakdown happens via shear and resonance [53, 54, 55], not through the usual process of destruction of homoclinic orbits. The primary results of the theoretical analysis are:

- The periodic fluctuation of debris charge in a flowing plasma leads to chaotic ion-acoustic oscillations and the chaos occurs through a phase of torus breakdown. This is substantiated by a KAM tori analysis.
- The reason why a periodically fluctuating negative debris charge induces a much weaker chaos than positive debris charge is due to the fluctuation forcing the system away from a dynamically stable configuration when the debris charge is positive.
- Through the FTLE maps, the theoretical analysis has also been able to show why the stochastic component affect the chaos only negligibly.

At the end, we have carried out an energy spectrum analysis of the chaotic phase space, which further confirms the dynamic stability of the nonlinear structures induced by negatively charged debris. Our work adds a new aspect to the science of the detection of LEO space debris. While existing methods leverage on plasma oscillations induced by the charged debris, the different chaotic signatures for positive and negatively charged debris as we have observed here add another layer to the detection scenario which can make the management of space debris even more robust.

Acknowledgement

BJ would like to acknowledge Gauhati University for research scholarship grant GU/UGC/GURF/2023/712. HS would like to thank CSIR-HRDG, New Delhi, India for Senior Research Fellowship research grant 09/059(0074)/2021-EMR-I.

The authors would also like to thank the anonymous referees as their critical comments and suggestion have greatly improved the manuscript.

Appendix A. Collisionality and kinetic simulation

It can be argued about the validity of the kinetic simulation in the light of the regime of collisionality. In this appendix, we establish the validity of the kinetic modeling taking consideration of the e - i collision by evaluating the Knudsen number. We can derive the Knudsen number (Kn) from the first principle in plasma considering the fact that the dominant collisions are between electrons and ions (this causes the highest momentum transfer). So, by definition, we have

$$\text{Kn} = \frac{\lambda_{\text{mean}}}{L}, \quad (\text{A.1})$$

where λ_{mean} is the mean free path for e - i collisions and L is the characteristic length of the system. As compared to the ions, electrons are highly mobile (in our case as well), we can assume that

$$\lambda_{\text{mean}} \simeq \frac{v_{\text{the}}}{\nu_{ei}}, \quad (\text{A.2})$$

where the electron thermal velocity, $v_{\text{the}} = \sqrt{T_e/m_e}$ and electron-ion collision frequency, ν_{ei} for Coulomb cross section can be approximated as [35]

$$\nu_{ei} \sim \frac{ne^4}{16\pi\epsilon_0^2 m_e^2 v_{\text{the}}^3}, \quad (\text{A.3})$$

where n is the average plasma density. Our simulation box is of length $L \sim 140\lambda_D \sim 1\text{ cm}$. Plugging all the numbers for our simulation parameters, we arrive at the value for the Knudsen number as

$$\text{Kn} \sim 15 \gg 1, \quad (\text{A.4})$$

which shows that the regime is almost collision-free and the use of kinetic theory is quite justified (through the PIC model).

It can further be argued about the use of the fluid model (Section 2.4) when $\text{Kn} \gg 1$. We note that the fluid equations used in this work (or in plasma physics contexts as well) are weighted average of the Boltzmann-Vlasov equation rather than the collisional Boltzmann equation (using Chapman-Enskog expansion). Naturally these fluid equations are valid *even* in the limit of zero collisions, which is due to the fact that the plasma dynamics is governed by long range Coulomb force rather than Newtonian collisional dynamics (like a hydrodynamic gas).

References

- [1] I. Langmuir, Phys. Rev. 21 (1923) 419.
- [2] H. M. Mott-Smith, I. Langmuir, Phys. Rev. 28 (1926) 727.
- [3] L. Tonks, I. Langmuir, Phys. Rev. 33 (1929) 195.
- [4] L. Tonks, I. Langmuir, Phys. Rev. 34 (1929) 876.
- [5] I. Langmuir, Phys. Rev. 33 (1954) (1929).
- [6] I. Langmuir, K. T. Compton, Rev. Mod. Phys. 3 (191) (1931).
- [7] E. C. Whipple, Rep. Prog. Phys. 44 (1981) 1197.
- [8] C. K. Goertz, W.-H. Ip, Geophys. Res. Lett. 11 (4) (1984) 349.
- [9] N. N. Rao, P. K. Shukla, M. Y. Yu, Planet. Space Sci. 38 (4) (1990) 543.
- [10] P. K. Shukla, A. A. Mamun, Introduction to dusty plasma physics, IOP, Bristol and Philadelphia, 2002.
- [11] J. F. Friichtenicht, Micrometeoroid impacts in space, NASA Technical Note NASA TN D-5750, NASA, Washington, D.C. (1969).
- [12] A. C. Tribble, The Space Environment: Implications for Spacecraft Design, Princeton University Press, 2004.
- [13] U. Samir, K. H. W. Jr., N. H. Stone, Rev. Geophys. 21 (7) (1983) 1631.
- [14] G. L. Delzanno, X.-Z. Tang, Phys. Plasmas 22 (2015) 113703.
- [15] J. Wang, X. Yue, F. Ding, B. Ning, L. Jin, C. Ke, et al., Radio Sci. 57 (12) (2022) e2022RS007472.
- [16] J. I. Murray, T. Kennedy, M. Matney, R. Miller, Radar observations from the haystack ultrawideband satellite imaging radar in 2019, in: 8th European Conference on Space Debris (ECOSD), Virtual (sponsored by ESA), 2021, NASA Technical Reports Server Document ID 20210011826; presents LEO debris measurements down to ~ 5.5 mm using HUSIR.
- [17] P. Bernhardt, L. Scott, A. Howarth, Modeling of plasma wave generation by orbiting space objects for proximity detection, AMOS Technical Conference Poster (Aug. 2023).
- [18] A. Sen, S. Tiwari, S. Mishra, P. Kaw, Adv. Space Res. 56 (3) (2015) 429–435.
- [19] S. Jaiswal, P. Bandyopadhyay, A. Sen, Phys. Plasmas 23 (8) (2016).
- [20] G. Arora, P. Bandyopadhyay, M. Hariprasad, A. Sen, Phys. Plasmas 26 (9) (2019).

- [21] H. Sarkar, M. P. Bora, Response of a dusty plasma system to external charge perturbations, *Physics of Plasmas* 30 (8) (2023).
- [22] H. Sarkar, M. P. Bora, *Phys. Plasmas* 32 (6) (2025).
- [23] M. Das, M. P. Bora, *Phys. Plasmas* 32 (2025) 032301.
- [24] A. S. Truitt, C. M. Hartzell, *J. Spacecraft Rockets* 57 (5) (2020) 876.
- [25] S. P. Acharya, A. Mukherjee, M. S. Janaki, *Phys. Rev. E* 104 (1) (2021) 014214.
- [26] A. S. Truitt, C. M. Hartzell, *J. Spacecraft Rockets* 57 (5) (2020) 975.
- [27] G. Ganguli, C. Crabtree, A. Fletcher, A. Sen, *Phys. Plasmas* 32 (2025) 022902.
- [28] M. R. Jana, A. Sen, P. K. Kaw, *Phys. Rev. E* 48 (1993) 3930.
- [29] G. Brodin, Nonlinear landau damping, *Phys. Rev. Lett.* 78 (7) (1997) 1263. doi:10.1103/PhysRevLett.78.1263.
- [30] H. Mushtaq, K. Singh, S. Zaheer, I. Kourakis, *Sci. Rep.* 14 (2024) 13005.
- [31] J. D. Meiss, *Differential Dynamical Systems*, SIAM, 2007.
- [32] N. Carlevaro, G. Montani, M. V. Falessi, *J. Plasma Phys.* 86 (4) (2020) 845860401.
- [33] C. Birdsall, A. Langdon, *Plasma Physics via Computer Simulation*, CRC Press, 2004.
- [34] J. P. Boris, D. L. Book, *J. Comput. Phys.* 11 (1973) 38.
- [35] F. F. Chen, *Introduction to plasma physics and controlled fusion*, 2nd Edition, Vol. 1, Plenum Press, New York and London, 1974.
- [36] S. Changmai, M. P. Bora, *Phys. Plasmas* 26 (2019) 042113.
- [37] S. Changmai, M. P. Bora, *Sci. Rep.* 10 (2020) 20980.
- [38] M. Das, S. Changmai, M. P. Bora, *Phys. Rev. E* 108 (2023) 045202.
- [39] P. H. Yoon, T. Rhee, C.-M. Ryu, *Phys. Plasmas* 12 (2005) 062310.
- [40] M. L. Nastac, R. J. Ewart, W. Sengupta, A. A. Schekochihin, M. Barnes, W. D. Dorland, *Phys. Rev. E* 109 (2024) 065210.
- [41] A. Mallet, K. G. Klein, B. D. G. Chandran, D. G. selj, I. W. Hoppock, T. A. Bowen, C. S. Salem, S. D. Bale, *J. Plasma Phys.* 85 (3) (2019) 175850302.
- [42] A. Wolf, J. B. Swift, H. L. Swinney, J. A. Vastano, *Phys. D: Nonlinear Phenom.* 16 (3) (1985) 285.

- [43] F. Takens, Detecting strange attractors in turbulence, in: D. A. Rand, L.-S. Young (Eds.), *Dynamical Systems and Turbulence*, Warwick 1980, Vol. 898 of *Lecture Notes in Mathematics*, Springer, 1981, pp. 366–381. doi:10.1007/BFb0091924.
- [44] H. Kantz, T. Schreiber, *Nonlinear Time Series Analysis*, 2nd Edition, Cambridge Nonlinear Science Series, Cambridge University Press, 2004.
- [45] S. T. Zalesak, *J. Comput. Phys.* 31 (3) (1979) 335.
- [46] J. L. Kaplan, J. A. Yorke, Chaotic behavior of multidimensional difference equations, in: H.-O. Peitgen, H.-O. Walther (Eds.), *Functional Differential Equations and Approximation of Fixed Points*, Vol. 730 of *Lecture Notes in Mathematics*, Springer, 1979, pp. 204–227. doi:10.1007/BFb0064316.
- [47] G. Strang, *Linear Algebra and Its Applications*, 4th Edition, Thomson Brooks/Cole, 2006.
- [48] J. P. Verboncoeur, *Plasma Phys. Control. Fusion* 47 (5A) (2005) A231.
- [49] J. M. Greene, *J. Math. Phys.* 20 (1979) 1183.
- [50] A. J. Lichtenberg, M. A. Lieberman, *Regular and Chaotic Dynamics*, 2nd Edition, Springer-Verlag, 1992.
- [51] V. I. Arnold, *Russ. Math. Surveys* 18 (5) (1963) 9.
- [52] S. H. Strogatz, *Nonlinear dynamics and chaos: with applications to physics, biology, chemistry, and engineering*, CRC Press, 2018.
- [53] C. Chandre, M. Govin, H. R. Jauslin, *Phys. Rev. E* 57 (1998) 1536.
- [54] D. Gaidashev, H. Koch, *Nonlinearity* 17 (2004) 1713.
- [55] K. Fuchss, A. Wurm, A. Apte, P. J. Morrison, *Chaos* 16 (2006) 033120.
- [56] S. C. Shadden, F. Lekien, J. E. Marsden, *Phys. D: Nonlinear Phenom.* 212 (2005) 271.
- [57] S. C. Shadden, Lagrangian coherent structures, in: R. Camassa, R. McLaughlin, J. Miles (Eds.), *Transport and Mixing in Laminar Flows: From Microfluidics to Oceanic Currents*, Wiley-VCH Verlag GmbH & Co., 2012, Ch. 3, pp. 59–89.
- [58] M. B. Isichenko, *Phys. Rev. Lett.* 78 (12) (1997) 2369.
- [59] C. Mouhot, C. Villani, *Acta Math.* 207 (1) (2011) 29.
- [60] J. L. Tennyson, J. D. Meiss, P. J. Morrison, *Phys. D: Nonlinear Phenom.* 71 (1-2) (1994) 1.
- [61] C. S. Kueny, P. J. Morrison, *Phys. Plasmas* 2 (1995) 4149.